Ore Geology Reviews 72 (2016) 179–190

Contents lists available at ScienceDirect

Ore Geology Reviews

journal homepage: www.elsevier.com/locate/oregeorev

Origin of the Luping Pb deposit in the Beiya area, Yunnan Province, SW China: Constraints from geology, isotope geochemistry and geochronology

Jia-Xi Zhou [a,b,*], Song Dou [b], Zhi-Long Huang [a], Yin-Liang Cui [b,c,**], Lin Ye [a], Bo Li [c], Ting Gan [a,d], Hai-Rui Sun [a,d]

[a] State Key Laboratory of Ore Deposit Geochemistry, Institute of Geochemistry, Chinese Academy of Sciences, Guiyang 550081, China
[b] Yunnan Non-ferrous Metals Geological Bureau, Kunming 650051, China
[c] Department of Land Resources Engineering, Kunming University of Science and Technology, Kunming 650093, China
[d] University of Chinese Academy of Sciences, Beijing 100049, China

ARTICLE INFO

Article history:
Received 13 November 2014
Received in revised form 21 July 2015
Accepted 21 July 2015
Available online 23 July 2015

Keywords:
Zircon U–Pb age
Alkaline porphyry
C–O–S and Pb isotopes
Luping epithermal Pb polymetallic deposit
Southwest China

ABSTRACT

The Luping Pb deposit, a newly discovered Pb–(Fe–Au–Ag–Zn) polymetallic deposit close to the Cenozoic Beiya porphyry-related Au–(Fe–Cu–Pb–Zn–Ag) deposit, is located in the central Sanjiang (three rivers: Jinshajiang, Lancangjiang and Nujiang) region (western Yangtze Block) in southwestern China. Ore bodies of the Luping deposit are mainly stratiform type, host in the Middle Triassic Beiya Formation limestone and Lower Triassic Qingtianbao Formation sandstone, and occur along NNW-trending bedding-plane faults within axis of Beiya–Qinghe syncline. Three ore types, namely the Pb–Au sulfide, Fe–Au, and Au ores, can be discerned regarding their ore metal association with reserves of 2.7 million tonnes (Mt) (average grade: 3.06 wt.% Pb, 0.66 g/t Au, 41 g/t Ag, and 0.82 wt.% Zn), 3 Mt (average grade: 30 wt.% Fe, 0.96 g/t Au and 31 g/t Ag), and 0.67 Mt (average grade: 2.16 g/t Au and 13 g/t Ag), respectively. Pb–Au sulfide ores contain mainly galena, siderite, native gold, sphalerite, and pyrite, with minor chalcopyrite, pyrrhotite and arsenopyrite, and gangue minerals such as quartz, calcite and dolomite. Sulfide ore textures include mainly brecciated, banded and vein, and minor massive and disseminated. LA-ICP-MS zircon U–Pb dating of alkali-rich quartz syenite porphyry from drill holes yielded a Late Eocene (Priabonian) age (36.2 ± 0.4 Ma), broadly coeval to the zircon U–Pb ages (ca. 38 Ma–31 Ma) of alkaline porphyries and molybdenite Re–Os age (36.9 ± 0.3 Ma) from the Beiya deposit near Luping. Calcite separates have $\delta^{13}C_{PDB}$ and $\delta^{18}O_{SMOW}$ values ranging from −5.8‰ to −5.1‰ (average: −5.6‰) and +13.2‰ to +14.7‰ (mean: +13.6‰), respectively, suggesting association with the mantle. The sulfides have a narrow range of $\delta^{34}S_{CDT}$ values (+0.8‰–+2.8‰, mean +1.8‰), which is similar to that of mantle-derived S (0 ± 3‰). $^{206}Pb/^{204}Pb$, $^{207}Pb/^{204}Pb$ and $^{208}Pb/^{204}Pb$ values of the sulfides range from 18.62 to 18.69, 15.66 to 15.70 and 38.92 to 39.08, respectively, similar to those of the porphyry whole-rock ($^{206}Pb/^{204}Pb_{36\ Ma}$ = 18.61–18.71, $^{207}Pb/^{204}Pb_{36\ Ma}$ = 15.64–15.77 and $^{208}Pb/^{204}Pb_{36\ Ma}$ = 38.88–39.32). Ore deposit geology and C–O–S–Pb isotopic data suggest that the sources of metals and ore-forming fluids were likely to be derived from the alkali-rich porphyries in the Beiya area. We propose that the Luping deposit is best classified as an epithermal Pb polymetallic deposit associated with the Beiya alkaline porphyries (ca. 36 Ma–31 Ma). Similar to other deposits related to the Cenozoic alkaline porphyries in the Jinshajiang–Red River (Ailaoshan) metallogenic belt, the Luping deposit may have been formed in the India–Eurasia post-collisional setting, when partial melting occurred in the Triassic stagnant slab that thickened the lower crust and the upper mantle, producing the alkaline magmatism and its associated mineralization.

1. Introduction

The Jinshajiang–Red River (Ailaoshan) fold belt (Fig. 1) (>1500 km long), is an important porphyry-related metallogenic belt in southwestern China (e.g., Deng et al., 2014; Hou et al., 2006, 2007; Hou and Cook, 2009; Wang et al., 2000, 2001). Distribution of alkaline intrusions and the porphyry-related Cu–Mo–(Au) and Pb–Zn–Ag deposits is controlled by the Jinshajiang–Red River (Ailaoshan) strike-slip fault system (e.g., Hou et al., 2007; Hu et al., 2004; Mao et al., 2014; Wang et al., 2001; Xu et al., 2012). Among these porphyry-related deposits, the Beiya skarn Au deposit is one of the most important and best studied (Fig. 1; Deng et al., 2015; Xu et al., 2006, 2007). The earliest Pb and Ag mining activities at Beiya can be dated back to the late

* Correspondence to: J.-X. Zhou, State Key Laboratory of Ore Deposit Geochemistry, Institute of Geochemistry, Chinese Academy of Sciences, Guiyang 550002, China.
** Correspondence to: Y.-L. Cui, Yunnan Non-ferrous Metals Geological Bureau, Kunming 650051, China.
E-mail addresses: zhoujiaxi@vip.gyig.ac.cn (J.-X. Zhou), cyl186@163.com (Y.-L. Cui).

http://dx.doi.org/10.1016/j.oregeorev.2015.07.015
0169-1368/

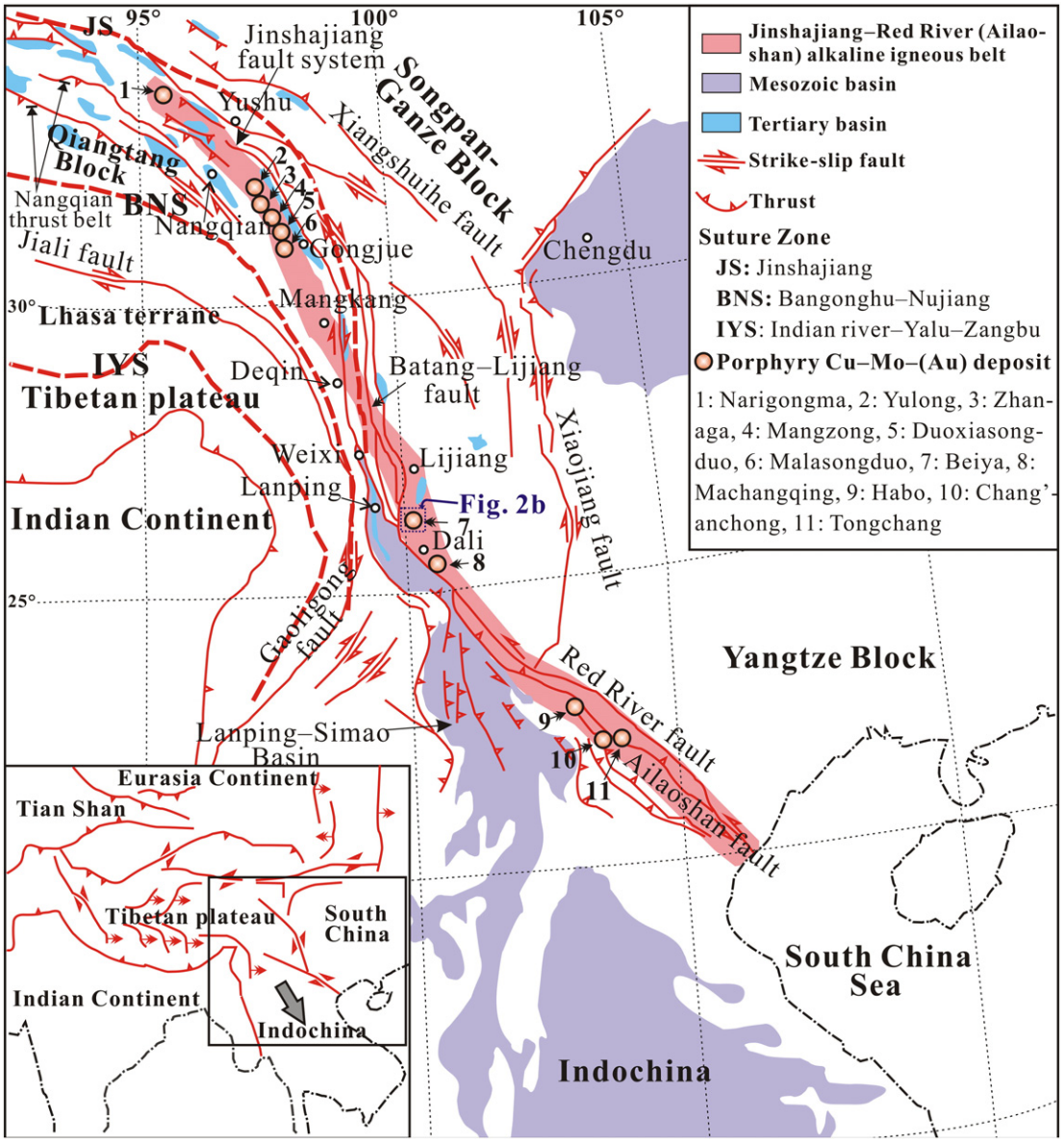

Fig. 1. Regional geological map showing the distribution of porphyry Cu–Mo–(Au) deposits along the Jinshajiang–Red River (Ailaoshan) fold belt. After Wang et al. (2001); Xu et al. (2012).

Ming dynasty (1368 — 1644 AD) (Cai, 1991). In the Beiya mineral district, five main types have been recognized (Xu et al., 2007): (i) porphyry Cu–Au, (ii) skarn Fe–Au, (iii) magmatic Fe–Au, (iv) sedimentary Au–Pb, and (v) paleo-placers Au associated with karsts. Among these five types, the skarn Fe–Au are the most important (Deng et al., 2015). The Luping deposit, a newly discovered Pb–(Fe–Au–Ag–Zn) deposit (Dou et al., 2013), is located one kilometer northwest of the Beiya Au deposit (Fig. 2a). Ore bodies in the Luping deposit are stratiform or lenticular sited along four concealed NNW-trending bedding-plane faults (Figs. 2b, 3 and 4) that are parallel to the bedding planes of the Beiya Formation limestone. The host rocks are the Middle Triassic Beiya Formation limestone and the Lower Triassic Qingtianbao Formation sandstone (Figs. 2b and 3). It was proposed to be a new type related to the alkaline porphyries in the Beiya area (Dou et al., 2013). However, due to the lack of isotopic and geochronological constraints, the sources of metals and ore-forming fluids, mineralization age and geodynamic setting are still unclear (Dou et al., 2013).

Isotopes, for example, C–O and S isotopes, are useful in determining the source of the ore-forming fluids (e.g., Bath et al., 2014; Mao et al., 2008; Moura et al., 2014; Palinkaš et al., 2013; Zhou et al., 2013a,b), whilst Pb isotopes have been widely used to constrain the source of the metals (e.g., Jemmali et al., 2013; Layton-Matthews et al., 2013; Pass et al., 2014; Zhou et al., 2014a,b). In this paper, we describe the geology of the Luping deposit and report new zircon U–Pb ages of the quartz syenite porphyry dikes, as well as new data of calcite C–O isotopes, sulfide S and Pb isotopes, and whole-rock Pb isotopes of the sedimentary host rocks and porphyries. With this new dataset, we will unravel the genetic links between the Luping deposit and the Beiya alkaline porphyries, and synthesize a new geodynamic model for the region.

2. Geological setting

2.1. Regional geology

A series of alkaline porphyries and many important porphyry-related Cu–Mo–(Au) and Pb–Zn–Ag deposits occur along the Jinshajiang suture in eastern Tibet. These alkaline porphyries and ore deposits were formed during the India–Eurasia collision, and constitute the famous Jinshajiang–Red River (Ailaoshan) alkali-rich porphyry-

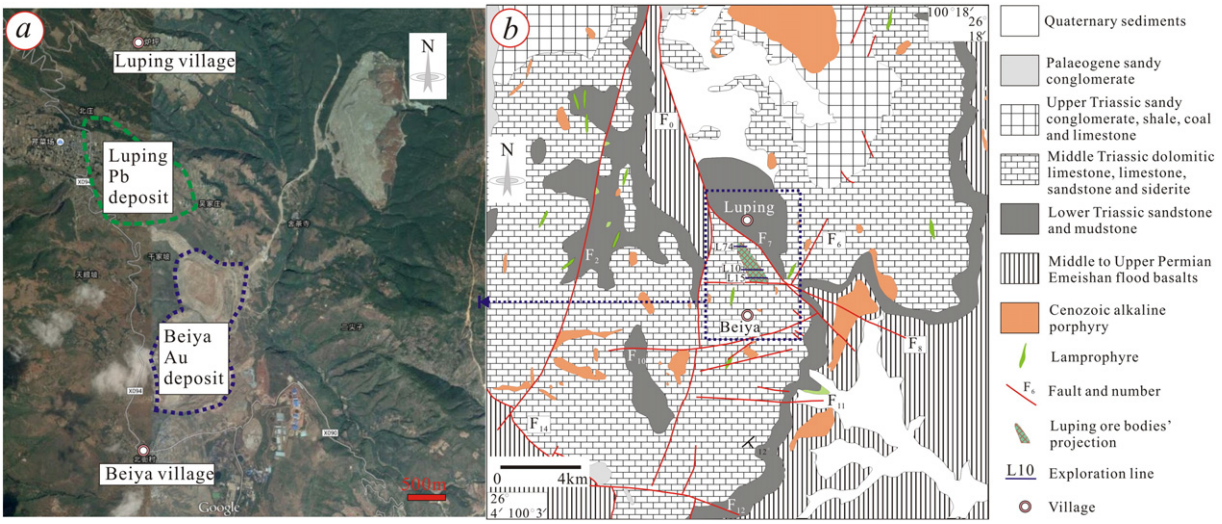

Fig. 2. a: Locations of the Luping Pb deposit and the Beiya Au deposit (Google map); b: Geological map of the Luping/Beiya area showing lithologies, structures and distribution of alkaline intrusions.
Modified from Dou et al. (2013).

related metallogenic belt (Fig. 1; Deng et al., 2014; Hou et al., 2006, 2007; Hou and Cook, 2009; Mao et al., 2014; Wang et al., 2001). Some of the important porphyry-related deposits along the belt include the Yulong Cu deposit (e.g., Hou et al., 2007; Zaw et al., 2007), the Beiya Au–Fe–Cu–Pb deposit (e.g., Deng et al., 2015; Xu et al., 2007), the Machangqing Cu–Mo–(Au) deposit (e.g., Hou et al., 2007; Hu et al., 1997; Peng et al., 1998), and the Yaoan Pb–Zn–Ag–Au deposit (e.g., Ge et al., 2002; Qian et al., 2000; Yang et al., 2002). The Beiya deposit is the largest skarn Au system in the region. The mineral district is located at the central part of this belt (Fig. 1) and is hosted by a porphyritic monzogranitic stock that is crosscut by porphyritic granite and later lamprophyre (Deng et al., 2015). At Beiya, major rock types include the Middle to Upper Permian Emeishan flood basalts, Lower Triassic Qingtianbao Formation sandstone and mudstone, Middle Triassic Beiya Formation limestone and sandstone, together with the sandy conglomerate, shale and limestone of the Upper Triassic Zhongwo and Songgui Formations. These rock sequences are then overlain by Paleogene sandy conglomerate and Quaternary sediments (Fig. 2b; Deng et al., 2015; Xu et al., 2007). The Beiya Formation strata are 550 m thick and are characterized by extensive karst formation, of which some caves and fissures are filled by sediments containing Fe oxides and porphyries lithic fragments (Xu et al., 2007). The Permian and Triassic rocks occur in an N-striking Cenozoic basement fault upon which is superimposed a broad N–S syncline (Fig. 2b). Abundant Tertiary porphyries are distributed in the Beiya area, including quartz-albite porphyry, quartz–K-feldspar porphyry, biotite–K-feldspar porphyry and lamprophyre (Deng et al., 2015; Xu et al., 2007). All the porphyries have similar ages (ca. 38 Ma–31 Ma) and geochemical features, including high alkalinity ($K_2O + Na_2O > 10$ wt.%), high silica ($SiO_2 > 65$ wt.%), high Sr (>400 ppm) and high $^{87}Sr/^{86}Sr$ values (>0.706) (e.g., Deng et al., 2015; He et al., 2013; Liu et al., 2015; Lu et al., 2012; Xu et al., 2006, 2007). At Luping, porphyries are not well-exposed (Fig. 2b) and are largely revealed by drill holes (Fig. 3).

2.2. Ore deposit geology of the Luping Pb deposit

2.2.1. Stratigraphy and lithology

At Luping, rocks exposed are the Middle to Upper Permian Emeishan basalts and Lower to Middle Triassic sedimentary rocks (Fig. 2b; Dou et al., 2013). The Middle Triassic Beiya Formation can be divided into a lower unit containing argillaceous limestone, siderite-bearing conglomeratic limestone and bioclastic limestone, and an upper unit containing dolomitic limestone and calcarenite (Figs. 2b and 3). Gold ore bodies are hosted in the Qingtianbao Formation sandstone, whereas the Pb–(Fe)–Au ore bodies are hosted in the Beiya Formation limestone (lower unit) (Figs. 2b and 3).

2.2.2. Structure

The regional NS-, NNW-, NW- and EW-trending structures are developed at Beiya (Fig. 2b; Deng et al., 2015; Xu et al., 2007), whereas WNW, NNW and NNE-trending structures are mainly present at Luping. These structures include the NNW-trending Beiya–Qinghe syncline (Fig. 2b), the NNW-trending Maanshan fault (F_0), the WNW-trending Jiaojiayuan–Wochanghe fault (F_8), and the NNE-trending Shechasi fault (F_6). Additionally, four concealed NNW-trending extensional bedding-plane faults (F_1, F_2, F_3 and F_4) within axis of the Beiya–Qinghe syncline were delineated from drill cores in the Luping deposit (Figs. 3 and 4). Quaternary sediments and the upper unit of the Beiya Formation form the core of the Beiya–Qinghe syncline, and the lower unit of the Beiya Formation and the Qingtianbao Formation form the limbs. Dip angles of the limbs are 10° –40° and 20°–50° in the eastern and western part, respectively (Dou et al., 2013). Dip angles of the four concealed bedding-plane faults are similar to those of sedimentary strata, from 5° to 25° (Figs. 3 and 4). The Luping deposit is located in the core of the Beiya–Qinghe syncline, and comprises four groups (Nos. I–IV) of stratiform or lenticular ore bodies (Figs. 3 and 4). These ore bodies occur along tectonic breccia belt-related to the bedding-plane faults (Figs. 3 and 4; Dou et al., 2013).

2.2.3. Ore body occurrence

No. I ore group occurs within the F_1 bedding-plane fault (Figs. 3 and 4) at 1770 m–1950 m levels. This group (1000 m long, 100 m–300 m wide and 1.5 m–45 m thick with dip angles of 5°–25°) (Figs. 3 and 4) contains 11 oxidized Pb–(Fe)–Au ore bodies, of which the I-1 ore body is the largest (Fig. 4). No. II ore group occurs within the F_2 bedding-plane fault (Figs. 3 and 4) at 1690 m–1840 m levels. This group (1540 m long, 300 m–450 m wide and 5 m–73.3 m thick with dip angles of 5°–15°) (Figs. 3 and 4) contains 13 oxidized Pb–(Fe)–Au ore bodies, of which the II-4 ore body is the largest (Fig. 4). No. III ore group occurs within the F_3 bedding-plane fault (Figs. 3 and 4) at 1550 m–1850 m levels. This group (2175 m long, 400 m–960 m wide and 20 m–98 m thick with dip angles of 5°–10°) (Figs. 3 and 4) contains 12 Pb–(Fe)–Au ore bodies with oxidized-sulfide mixed ores. In the No. III ore group, the III-1 ore body is the largest (2175 m long, 505 m wide and 6.15 m thick) (Fig. 4). It contains at least 1.17 Mt oxidized-sulfide mixed ores with average grades of 3.43 wt.% Pb, 0.68 g/t Au, 48 g/t Ag

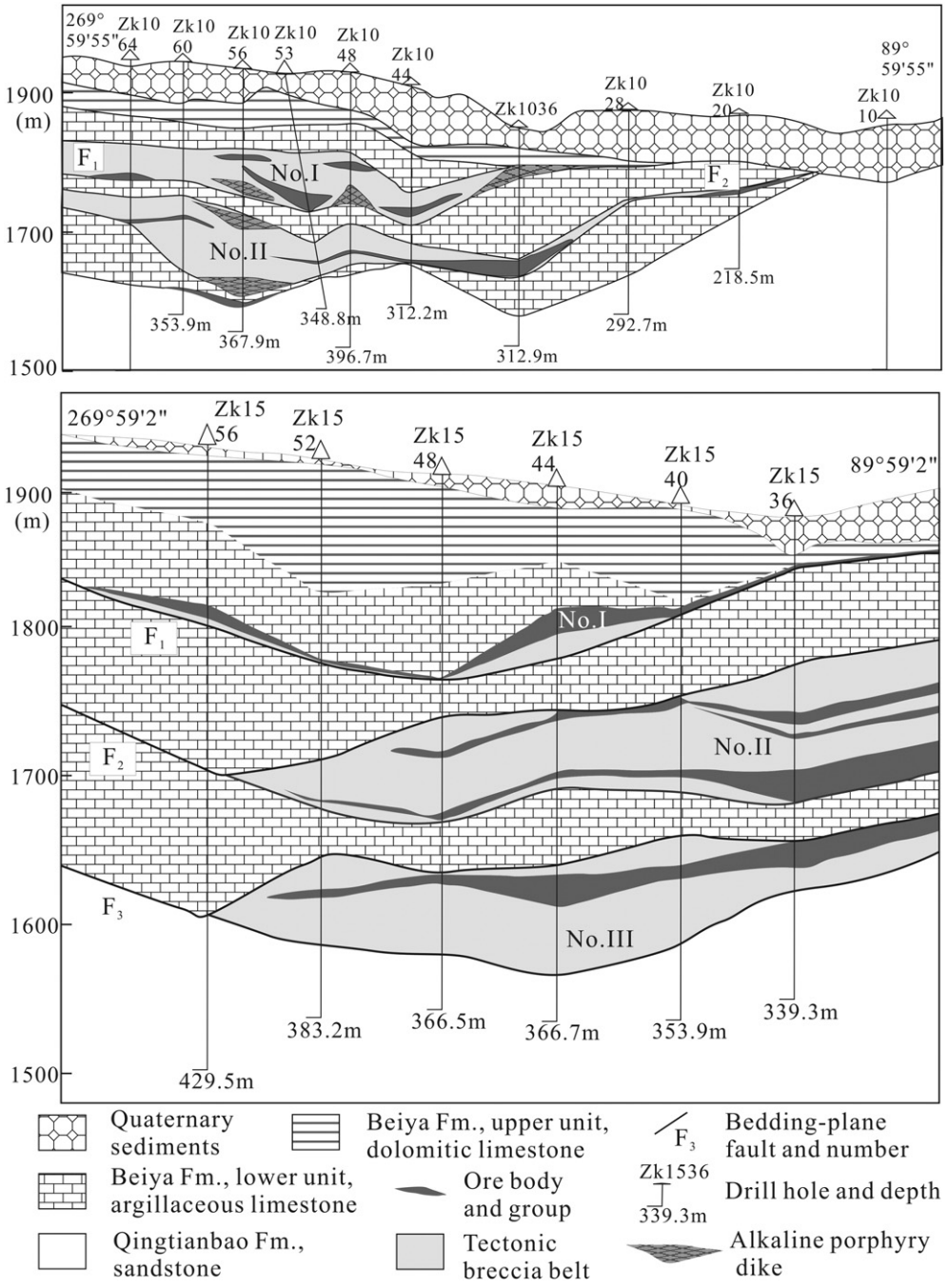

Fig. 3. Cross–section maps of Nos. 10 and 15 exploration lines in the Luping Pb deposit showing the drill holes, ore bodies, porphyry dikes, ore–controlling faults and wall rock lithologies. Modified from Dou et al. (2013).

and 0.84 wt.% Zn. No. IV ore group occurs within the F_4 bedding-plane fault (Figs. 3 and 4) at 1550 m–1750 m levels. This group (1720 m long, 50 m–250 m wide and 1.5 m–9.58 m thick with dip angles of 5°–15°) (Figs. 3 and 4) contains 3 Au ore bodies with primary ores, of which the IV-3 ore body is the largest (Fig. 4). At Luping, mineralization zonation shows generally Fe–Au metal assemblage in the southeast and Pb–Au metal assemblage in the northwest. At depths, Pb–Au occurs above Fe–Au, which in turn occurs above Au (Fig. 4; Dou et al., 2013).

2.2.4. Texture and structure of the ores

Ores at Luping have undergone skarn and hydrothermal alteration, and supergene oxidation. Therefore, there are primary (sulfide and Fe minerals), secondary and mixed ores, of which the Pb–(Fe)–Au oxidized and sulfide ores predominate. Pb–Au sulfide ores mainly comprise of galena, native gold and electrum, with minor sphalerite, chalcopyrite, pyrite, pyrrhotite and arsenopyrite. Primary Fe–Au ores mainly consist of magnetite, siderite, native gold and electrum. Oxidized and mixed ores have extremely complex mineral assemblages of magnetite, cerussite, limonite, smithsonite, massicot (PbO), malachite, native gold and sulfide minerals (Fig. 5a, b, c).

The Pb–Au sulfide ores show mainly brecciated, banded and vein structures, and minor massive and disseminated styles (Figs. 5d, e, f, g, h, i and 6a, b, c, d). Minerals show various textures in different ore types. For example, in brecciated ores, pyrite is fine-grained (0.2 mm–1 mm) euhedral and chalcopyrite is coarse-grained (2 mm–8 mm) anhedral. In banded ores (Figs. 5e, i and 6b), galena is fine-grained (0.02 mm–0.2 mm) euhedral and occurs as aggregates (2 mm–4 mm), and siderite is coarse-grained euhedral in veins (5 mm–20 mm wide).

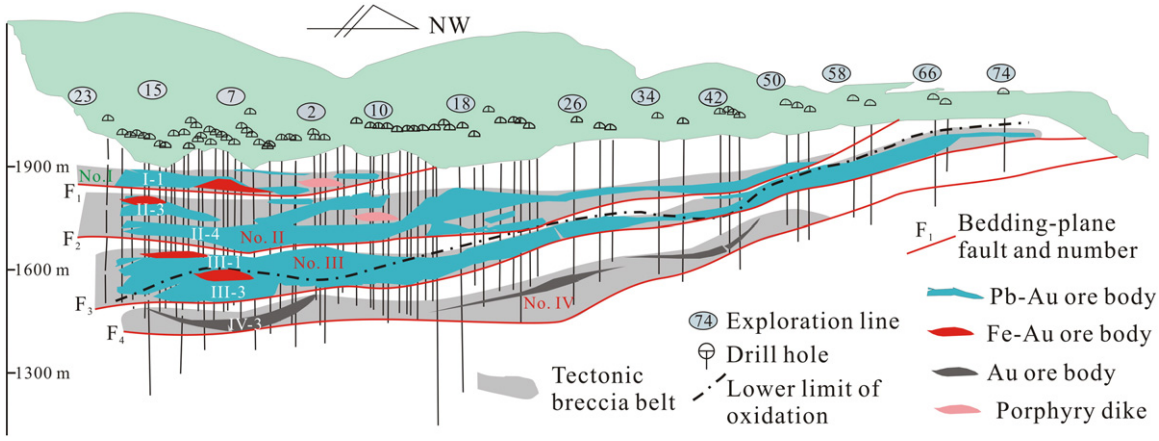

Fig. 4. Spatial distribution of ore bodies at Luping.
Modified from Dou et al. (2013).

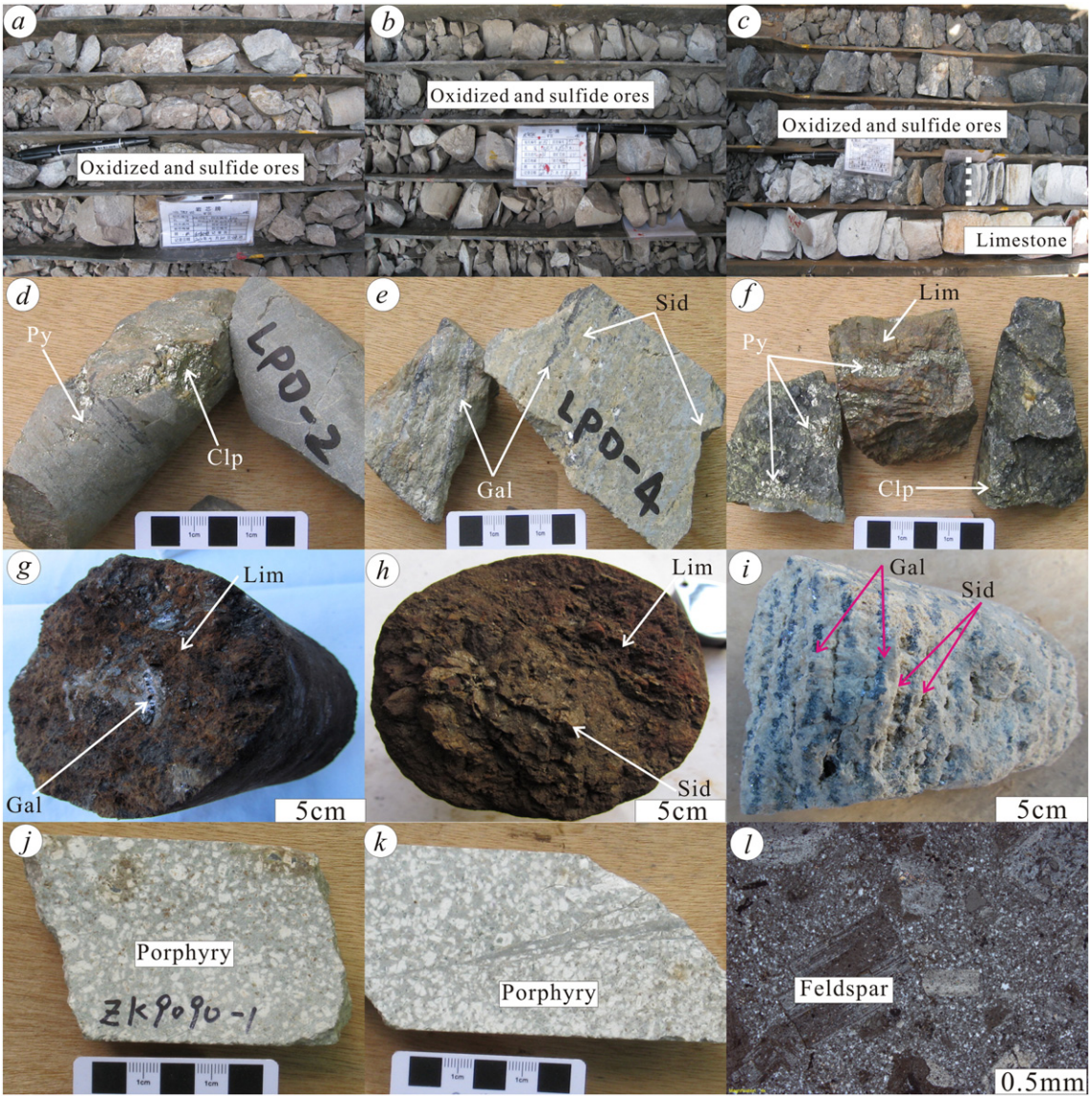

Fig. 5. a–c: Oxidized and sulfide ores revealed by drilling; c: Contacts between ores and limestone; d: Disseminated pyrite (Py) and chalcopyrite (Clp) assemblage in limestone; e: Banded galena (Gal) within banded siderite (Sid); f: Disseminated Py and Clp within limonite (Lim); g: Granular Gal assemblage in Lim; h: Granular Sid assemblage is coexist with brecciated Lim assemblage; i: Banded Gal within banded Sid; j–k: Porphyries revealed by drill holes; l: Feldspar phenocryst in porphyries.

In ore veins (Fig. 6c, d), galena is fine- to coarse-grained (0.06 mm–4 mm) anhedral to euhedral and fills in siderite, which is coarse-grained (2 mm–6 mm) euhedral.

2.2.5. Mineral paragenesis

At Luping, the skarn, hydrothermal and supergene mineralization represent the three major metallogenic phases, of which the hydrothermal phase dominates. Ore and gangue minerals formed in the skarn phase include garnet, diopside, magnetite, pyrite, quartz and native gold. The hydrothermal phase can be divided into the Fe–Au and Pb–Au stages. Major minerals formed in the Fe–Au stage include siderite, pyrite, chalcopyrite, quartz and native gold (Fig. 5d). Based on crosscutting, overgrowth and replacement relationships, the calcite and galena in the Pb–Au stage can be divided into three sub-stages (Figs. 5 and 6; Dou et al., 2013). The paragenetic sequence of the Luping deposit is shown in Table 1 and Figs. 5 and 6.

2.2.6. Wall rock alteration

Skarnization at Luping has formed garnet, diopside and magnetite with associated Fe–Au mineralization. Wall rock alteration styles in the hydrothermal stage are complex, and include pyritization, silicification, and carbonatization (Dou et al., 2013). Pyritization usually occurs in the Beiya Formation limestone and the Qingtianbao Formation sandstone with associated Pb–Au mineralization. The Beiya Formation limestone shows weak silicification, but the Qingtianbao Formation sandstone has stronger silicification and is associated with Au mineralization. Carbonatization (calcite, dolomite and siderite) is commonly associated with Au polymetallic mineralization at Luping (Beiya) (Dou et al., 2013; Xu et al., 2007).

2.2.7. Igneous rocks

Quartz syenite porphyry dikes were intersected by drill holes at Luping (Fig. 3a). These concealed porphyry dikes occur in the concealed bedding-plane faults within axis of the Beiya–Qinghe syncline and are spatially associated with Pb–(Fe)–Au ore bodies (Figs. 3a and 4). The porphyries contain mainly quartz and feldspar phenocrysts (Fig. 5j, k, l). Whole-rock geochemistry of the porphyry shows potassic and adakite-like characteristics, as evidenced by high alkalinity ($K_2O + Na_2O > 10$ wt.%), and high K_2O/Na_2O (5–28), Sr/Y (17–91) and $(La/Yb)_N$ (17–34) values (Dou et al., 2013). Petrologic and lithogeochemical characteristics of the quartz syenite porphyry dikes at Luping are similar to those of the alkaline porphyries at Beiya (e.g., Deng et al., 2015; Dou et al., 2013; He et al., 2012; Liu et al., 2015; Xu et al., 2006, 2007).

3. Samples and analytical methods

Twenty-seven representative sulfide ore samples from the major Pb–Au ore bodies were collected from drill cores. Pyrite ($n = 4$), sphalerite ($n = 1$), galena ($n = 9$), and calcite ($n = 8$) separates from the main metallogenic stage were hand-picked from using a binocular microscope and were subsequently analyzed for C–O, S and Pb isotopes. In addition, whole-rock samples ($n = 13$) of the Beiya and Qingtianbao Formations sedimentary rocks and porphyries were analyzed for Pb isotopes. One quartz syenite porphyry sample (ZK9090) was zircon U–Pb dated.

3.1. Zircon LA-ICP-MS U–Pb dating

Zircon grains were separated from about 2 kg of quartz syenite porphyry sample (ZK9090) using standard density and magnetic separation techniques at the Geological Laboratory of Hebei Province, China. Internal structure was examined using cathodoluminescence (CL) prior to U–Pb isotope analysis. U–Pb dating was undertaken at the State Key Laboratory of Ore Deposit Geochemistry, Chinese Academy of Sciences, using the laser ablation inductively coupled plasma mass spectrometer (LA-ICP-MS). U–Pb ages were calculated using the program ICP-MS Data-Cal (Liu et al., 2008, 2010a). Detailed analytical procedures are available in Liu et al. (2008, 2010a,b).

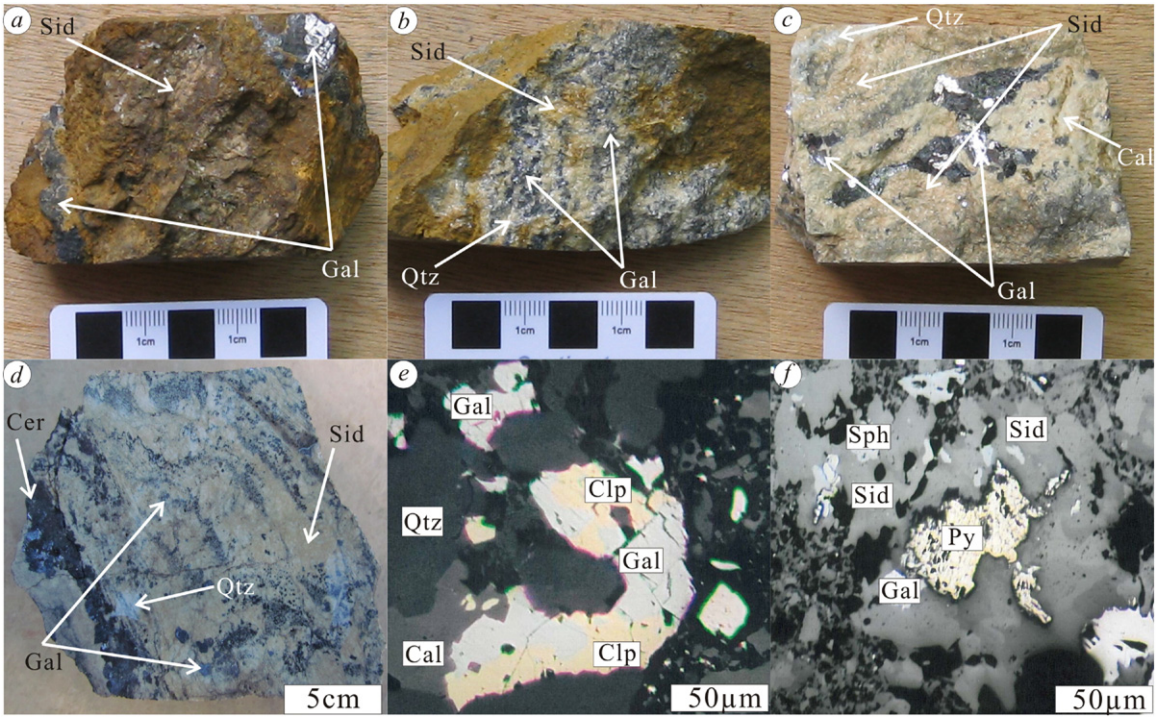

Fig. 6. a: Granular galena (Gal) enclosed in siderite (Sid); b: Quartz (Qtz) in banded Sid and Gal; c: Granular Gal, calcite (Cal) and Qtz assemblages enclosed in Sid; d: Vein and disseminated Gal and cerussite (Cer) together with massive Sid; e: Chalcopyrite (Clp) within Gal, coexisting with Qtz and Cal, Gal metasomatic relict Clp; f: Sphalerite (Sph), Py and Gal together with Sid, Py eutectic boundary with Gal and Sid.

Table 1
Paragenetic sequence of the Luping deposit.

Period	Skarn	Hydrothermal		Supergene
Stage	Skarn stage	Fe–Au stage	Pb–Au stage	
Garnet				
Diopside				
Magnetite				
Pyrite				
Native Au				
Electrum				
Siderite				
Chalcopyrite				
Galena				
Sphalerite				
Arsenopyrite				
Pyrrhotite				
Quartz				
Calcite				
Dolomite				
Cerusite				
Limonite				
Smithsonite				
Massicottite				
Malachite				

3.2. Carbon and oxygen isotope analysis

$\delta^{13}C$ and $\delta^{18}O$ values were obtained using a Finnigan MAT-253 mass spectrometer at the State Key Laboratory of Environmental Geochemistry, Chinese Academy of Sciences. Calcite reacted with pure phosphoric acid to produce CO_2. The analytical precisions (2σ) are $\pm 0.2‰$ for $\delta^{13}C$ value and $\pm 0.5‰$ for $\delta^{18}O$ value. $\delta^{13}C$ and $\delta^{18}O$ values are reported relative to the Vienna Pee Dee Belemnite (V-PDB) and Vienna Standard Mean Ocean Water (V-SMOW), respectively.

3.3. Sulfur isotope analysis

Sulfur isotope analysis was undertaken at the State Key Laboratory of Environmental Geochemistry, Chinese Academy of Sciences, by using continuous flow isotope ratio mass spectrometer (CF-IRMS). GBW 04415 and GBW 04414 Ag_2S were used as external standards and the Vienna Canyon Diablo Troilite (V-CDT) as reference standard, with an analytical precision of $\pm 0.2‰$ (2σ).

3.4. Lead isotope analysis

Lead isotope analysis was carried out using a GV Isoprobe-T thermal ionization mass spectrometer (TIMS) at the Beijing Institute of Uranium Geology. The analytical procedure involved dissolution of samples using HF and $HClO_4$ in crucibles, followed by basic anion exchange resin to purify Pb. Analytical results for the standard NBS 981 are $^{206}Pb/^{204}Pb = 16.938 \pm 0.003$ (2σ, $n = 10$), $^{207}Pb/^{204}Pb = 15.456 \pm 0.004$ (2σ, $n = 10$) and $^{208}Pb/^{204}Pb = 36.612 \pm 0.005$ (2σ, $n = 10$).

4. Analytical results

4.1. LA-ICPMS zircon U–Pb ages

Zircon U–Pb analytical results of the quartz syenite porphyry are listed in Table 2 and illustrated on a concordia plot (Fig. 7b). The analyzed zircons are mostly transparent and idiomorphic crystals with igneous oscillatory zoning (Fig. 7a). Zircon grains of the Luping porphyry have high and uniform concentrations of U and Th (798 ppm–1904 ppm and 247 ppm–480 ppm, respectively). Their Th/U ratios (0.15–0.36, all > 0.1) are typical of magmatic origin. These zircon grains have concordant to nearly concordant U–Pb ages. Eight analyses have $^{206}Pb/^{238}U$ ages of 36.6 Ma–35.4 Ma with a weighted average $^{206}Pb/^{238}U$ age of 36.2 ± 0.4 Ma (2σ, MSWD = 1.6) (Fig. 7c).

4.2. Carbon and oxygen isotopic compositions

$\delta^{13}C_{PDB}$ and $\delta^{18}O_{SMOW}$ values of calcite separates are listed in Table 3 and shown in Fig. 8. Calcite separates have $\delta^{13}C_{PDB}$ and $\delta^{18}O_{SMOW}$ values ranging from −5.8‰ to −5.1‰ (average −5.6‰, $n = 8$) and +13.2‰ to +14.7‰ (average +13.6‰, $n = 8$), respectively.

4.3. Sulfur isotopic compositions

$\delta^{34}S_{CDT}$ values of sulfide separates are given in Table 4 and shown in Fig. 9a. Pyrite separates have a narrow range of $\delta^{34}S_{CDT}$ values of +2.3‰–+2.8‰ (average +2.6‰, $n = 4$). Sphalerite separate has a $\delta^{34}S_{CDT}$ value of +2.7‰. Galena separates have $\delta^{34}S_{CDT}$ values ranging from +0.8‰ to +1.8‰ (mean +1.3‰, $n = 9$). Thus, the $\delta^{34}S$ values of pyrite and sphalerite separates are higher than those of galena.

4.4. Lead isotopic compositions

Lead isotopic compositions of sulfides, sedimentary rocks and porphyries are listed in Table 5 and shown in Fig. 10. Pyrite separates have $^{206}Pb/^{204}Pb$ ratios ranging from 18.632 to 18.675, $^{207}Pb/^{204}Pb$ ratios ranging from 15.657 to 15.699 and $^{208}Pb/^{204}Pb$ ratios ranging from 38.923 to 39.084. $^{206}Pb/^{204}Pb$, $^{207}Pb/^{204}Pb$ and $^{208}Pb/^{204}Pb$ ratio for sphalerite separate is 18.694, 15.703 and 39.073, respectively.

Table 2
Zircon LA-ICP-MS U–Pb analysis results of quartz syenite porphyry at Luping.

No.	U/ppm	Th/ppm	Th/U	Isotope ratio				Model age/Ma			Source
				$^{207}Pb/^{206}Pb \pm 1\sigma$	$^{207}Pb/^{235}U \pm 1\sigma$	$^{206}Pb/^{238}U \pm 1\sigma$	$^{208}Pb/^{232}Th \pm 1\sigma$	$^{207}Pb/^{235}U \pm 1\sigma$	$^{206}Pb/^{238}U \pm 1\sigma$	$^{208}Pb/^{232}Th \pm 1\sigma$	
1	1177	415	0.35	0.04605 ± 0.00100	0.03619 ± 0.00073	0.00570 ± 0.00004	0.00194 ± 0.00010	36.1 ± 0.7	36.6 ± 0.3	39 ± 2	This
2	841	276	0.33	0.04611 ± 0.00368	0.03540 ± 0.00028	0.00557 ± 0.00007	0.00178 ± 0.00014	35.0 ± 3.0	35.8 ± 0.4	36 ± 3	paper
3	798	247	0.31	0.04605 ± 0.00521	0.03569 ± 0.00042	0.00562 ± 0.00007	0.00194 ± 0.00028	36.0 ± 4.0	36.1 ± 0.4	39 ± 6	
4	1038	374	0.36	0.04702 ± 0.00432	0.03648 ± 0.00033	0.00563 ± 0.00006	0.00179 ± 0.00012	36.0 ± 3.0	36.2 ± 0.4	36 ± 2	
5	1904	295	0.15	0.04704 ± 0.00626	0.03691 ± 0.00086	0.00569 ± 0.00011	0.00181 ± 0.00041	37.0 ± 5.0	36.6 ± 0.7	37 ± 8	
6	1280	480	0.38	0.04605 ± 0.00174	0.03500 ± 0.00026	0.00551 ± 0.00006	0.00201 ± 0.00019	35.0 ± 1.0	35.4 ± 0.4	41 ± 4	
7	1087	364	0.33	0.04605 ± 0.00602	0.03560 ± 0.00064	0.00561 ± 0.00007	0.00184 ± 0.00034	36.0 ± 5.0	36.0 ± 0.4	37 ± 7	
8	951	314	0.33	0.04605 ± 0.00355	0.03620 ± 0.00076	0.00570 ± 0.00006	0.00184 ± 0.00030	36.0 ± 3.0	36.6 ± 0.4	37 ± 6	

Galena separates have $^{206}Pb/^{204}Pb$, $^{207}Pb/^{204}Pb$ and $^{208}Pb/^{204}Pb$ ratios ranging from 18.623 to 18.657, 15.667 to 15.691 and 38.955 to 39.053, respectively. Pyrite, sphalerite and galena separates have similar Pb isotopes, suggesting similar source region. Whole-rock analyses of the Triassic Beiya and Qingtianbao Formations have yielded age-corrected (36 Ma) $^{206}Pb/^{204}Pb$, $^{207}Pb/^{204}Pb$ and $^{208}Pb/^{204}Pb$ ratios ranging from 18.659 to 18.908, 5.624 to 15.702 and 38.848 to 39.095, respectively. Porphyries whole-rock analyses have yielded age-corrected (36 Ma) $^{206}Pb/^{204}Pb$, $^{207}Pb/^{204}Pb$ and $^{208}Pb/^{204}Pb$ ratios ranging from 18.612 to 18.714, 15.636 to 15.771 and 38.884 to 39.315, respectively. It is clear that the sulfide separates data points fall into the field between the ore-hosting sedimentary rocks and porphyries in the $^{207}Pb/^{204}Pb$ vs. $^{206}Pb/^{204}Pb$ diagram (Fig. 10).

5. Discussion

5.1. Timing of alkaline porphyry and polymetallic mineralization

Our LA-ICP-MS zircon U–Pb age of 36.2 ± 0.4 Ma (Fig. 7b, c) for the quartz syenite porphyry dikes at Luping lies within the age range of alkaline porphyries at Beiya (ca. 38 Ma–31 Ma) (Deng et al., 2015; He et al., 2012, 2013; Liang et al., 2007; Liu et al., 2015; Lu et al., 2012; Zhang et al., 2000) and the Jinshajiang–Red River (Ailaoshan) belt (ca. 38 Ma–31 Ma) (e.g., Deng et al., 2014; Lu et al., 2012; Mao et al., 2014; Xu et al., 2007, 2014; Zhu et al., 2013).

Studies indicate that porphyry-related Cu–Mo–(Au) and epithermal Pb–Zn–Ag deposits in the Jinshajiang–Red River (Ailaoshan) belt formed at ca. 36 Ma–33 Ma (e.g., Deng et al., 2014, 2015; Hou et al., 2007; Hou and Zhang, 2015; Mao et al., 2014). He et al. (2013) reported a molybdenite Re–Os age of 36.9 ± 0.3 Ma from Beiya, which lies in the age range of alkaline porphyries emplacement at Beiya (ca. 38 Ma–31 Ma) and Luping (36.2 ± 0.4 Ma). Ore deposit geology (Figs. 2b and 3) and C–O–S–Pb isotopes (Figs. 8, 9 and 10) suggest that the Luping deposit is genetically linked to Eocene alkaline porphyries in the Beiya area. Therefore, we propose that the Luping deposit may have formed at ca. 36 Ma–31 Ma, most likely at 34 ± 2 Ma and associated with the alkaline porphyries at Beiya, similar to the other deposits (such as Yaoan) related to the alkaline porphyry system along the Jinshajiang–Red River (Ailaoshan) porphyry metallogenic belt (e.g., Deng et al., 2014, 2015; He et al., 2013; Hou et al., 2007; Lu et al., 2012; Mao et al., 2014; Zhang et al., 2000). This is also similar to the porphyry Cu and epithermal systems in the Dexing area in eastern China (Mao et al., 2011).

Table 3
C-O isotopic compositions of calcite separates from Luping and Beiya.

No.	Mineral	$\delta^{13}C_{PDB}$/‰	2σ	$\delta^{18}O_{SMOW}$/‰	2σ	Source
LPD-1	Calcite	−5.7	0.1	+13.8	0.1	This paper
LPD-3	Calcite	−5.1	0.1	+14.7	0.2	
LPD-4	Calcite	−5.8	0.2	+13.5	0.1	
LPD-10	Calcite	−5.7	0.1	+13.3	0.1	
LPD-19	Calcite	−5.8	0.2	+13.4	0.1	
LPD-27	Calcite	−5.5	0.1	+13.9	0.1	
LPD-26	Calcite	−5.7	0.1	+13.2	0.2	
LPD-29	Calcite	−5.6	0.2	+13.3	0.3	
The Beiya deposit	Stage I calcite	−8.1 to −5.1 ($n = 6$)		+11.6–+15.2 ($n = 6$)		Wu et al. (2010)
	Stage II calcite	−4.8 to −2.9 ($n = 6$)		+13.0–+15.9 ($n = 6$)		
	Stage III calcite	−1.1–+0.1 ($n = 3$)		+14.7–+18.7 ($n = 3$)		
	Marble	−0.8 – +0.7 ($n = 4$)		+23.8–+28.4 ($n = 4$)		

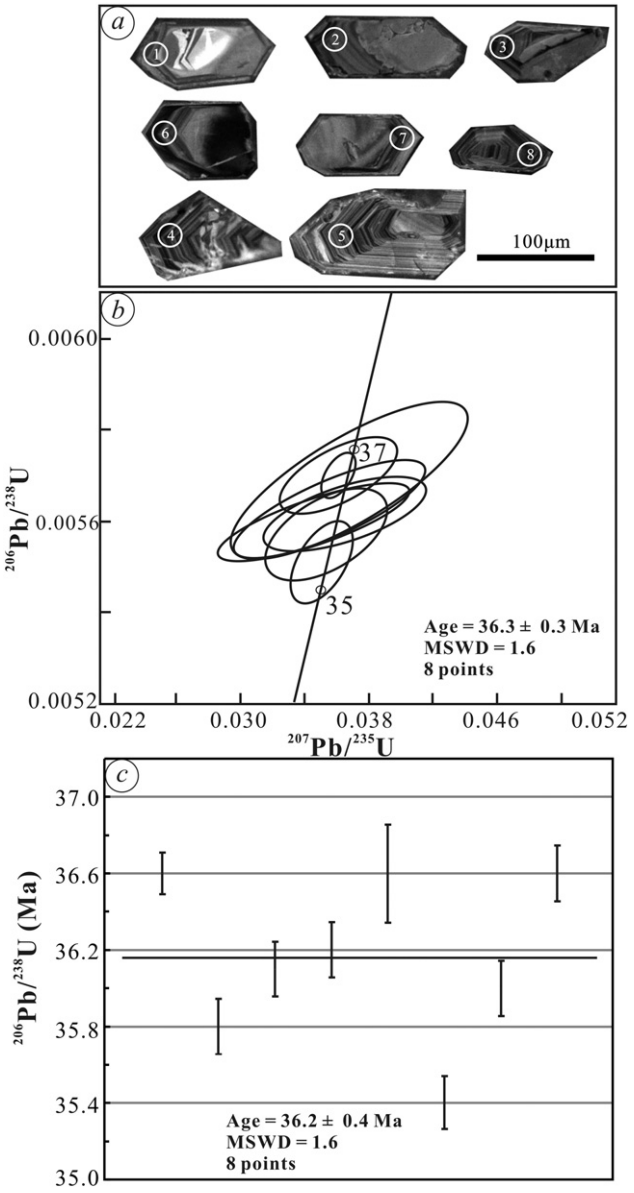

Fig. 7. a: CL images of the U–Pb dated zircons; b: U–Pb concordia diagram; c: Weighted average $^{206}Pb/^{238}U$ age.

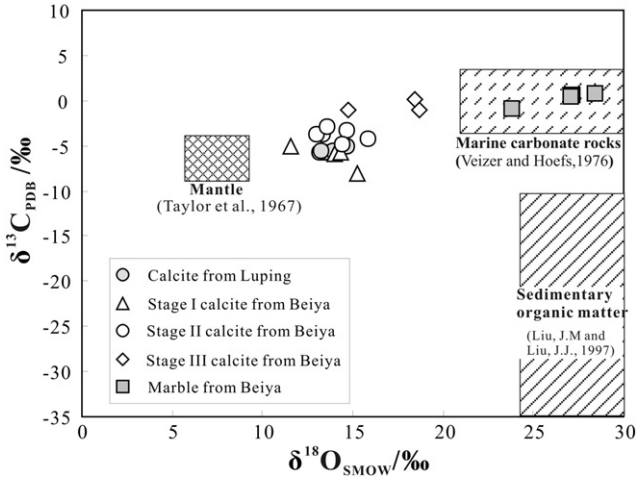

Fig. 8. Plot of $\delta^{13}C_{PDB}$ versus $\delta^{18}O_{SMOW}$ values for calcite and marble from the Luping and Beiya (Wu et al., 2010) deposits.

Table 4
S isotopic compositions of sulfide separates from Luping and Beiya.

No.	Mineral	$\delta^{34}S_{CDT}$/‰	2σ	Source
LPD-1	Pyrite	+2.3	0.2	This paper
LPD-2	Pyrite	+2.8	0.1	
LPD-18	Pyrite	+2.6	0.1	
LPD-28	Pyrite	+2.8	0.2	
LPD-10	Sphalerite	+2.7	0.1	
LPD-3	Galena	+1.8	0.1	
LPD-4	Galena	+1.3	0.1	
LPD-9	Galena	+0.8	0.1	
LPD-16	Galena	+0.9	0.2	
LPD-19	Galena	+1.1	0.1	
LPD-24	Galena	+1.1	0.1	
LPD-27	Galena	+1.1	0.2	
LPD-29	Galena	+1.7	0.2	
LPD-36	Galena	+1.7	0.1	
The Beiya deposit	Pyrite	−1.6–+4.5 ($n = 24$)		Xiao et al. (2011)
	Galena	−2.4–+1.8 ($n = 13$)		

5.2. Possible sources of ore-forming fluids

In general, carbon in hydrothermal fluids can be derived from the mantle, marine carbonate rocks or sedimentary organic matters (e.g., Demény et al., 1998; Demény and Harangi, 1996; Liu and Liu, 1997; Taylor et al., 1967; Veizer and Hoefs, 1976). The mantle, marine carbonates and organic matters have $\delta^{13}C_{PDB}$ and $\delta^{18}O_{SMOW}$ values of −4.0‰ to −8.0‰ and +6.0‰ to +10.0‰ (Taylor et al., 1967), −4.0‰ to +4.0‰ and +20.0‰ to +30.0‰ (Veizer and Hoefs, 1976), and −30.0‰ to −10.0‰ and +24.0‰ to +30.0‰ (Liu and Liu, 1997), respectively. In the $\delta^{13}C_{PDB}$ vs. $\delta^{18}O_{SMOW}$ diagram (Fig. 8), calcite separates from Luping fall into the area between the marine carbonate rocks and the mantle fields, and close to the mantle field. Meanwhile, the $\delta^{13}C_{PDB}$ values of calcite separates are higher than those of typical organic matters, lower than those of typical marine carbonates, and similar to those of the average mantle (Fig. 8). This indicates that carbonates and organic material did not contribute much C to the Luping hydrothermal fluids. The $\delta^{18}O_{SMOW}$ values plot in the area between the mantle and marine carbonates fields (Fig. 8), and far from the mantle field. This suggests that carbonates provide a certain amount of O to the Luping hydrothermal fluids, and O isotopes were partially in thermal equilibrium with the carbonate host rocks (Gray et al., 1991; Muchez et al., 1995). Wu et al. (2010) reported that the pre-mineralization (Stage I) calcite separates from Beiya have $\delta^{13}C_{PDB}$ values ranging from −8.1‰ to −5.1‰ ($n = 6$) and $\delta^{18}O_{SMOW}$ values from +11.6‰ to +15.2‰ ($n = 6$). Calcite separates from the main metallogenic stage (Stage II) have $\delta^{13}C_{PDB}$ and $\delta^{18}O_{SMOW}$ values ranging from −4.8‰ to −2.9‰ ($n = 6$) and from +13.0‰ to +15.9‰ ($n = 6$), respectively. The $\delta^{13}C_{PDB}$ and $\delta^{18}O_{SMOW}$ values of the post-mineralization (Stage III) calcite separates are −1.1‰ to +0.1‰ ($n = 3$) and +14.7‰ to +18.7‰ ($n = 3$), respectively. It is clear that calcite separates from Luping have $\delta^{13}C_{PDB}$ and $\delta^{18}O_{SMOW}$ values similar to those of the Stages II calcite separates from Beiya (Fig. 8; Wu et al., 2010). Therefore, C and O in the Luping ore-forming fluids were most likely to be derived from magma with limited contribution from the carbonate host rocks (Wu et al., 2010). The Stage III calcite separates from Beiya (Wu et al., 2010; Xiao et al., 2011) have $\delta^{13}C_{PDB}$ and $\delta^{18}O_{SMOW}$ values higher than those of Luping, suggesting that the carbonate host rocks may have provided more C and O for the Beiya ore-forming fluids in the late stage (Fig. 8).

Major Pb–Au primary ores at Luping have simple sulfide mineral assemblage, i.e., sphalerite, pyrite and galena. Therefore, the sulfide $\delta^{34}S$ values can act as a proxy for the $\delta^{34}S$ values of the ore-forming fluids (e.g., Basuki et al., 2008; Dixon and Davidson, 1996; Ohmoto et al., 1990; Ohmoto and Goldhaber, 1997; Ohmoto and Rye, 1979). All sulfide separates from Luping have $\delta^{34}S_{CDT}$ values ranging from +0.8‰ to +2.8‰ (Table 4), similar to mantle-derived S (0 ± 3‰; Chaussidon et al., 1989). Pyrite and galena separates (Xiao et al., 2011) from Beiya have $\delta^{34}S$ values (Table 4 and Fig. 9b) ranging from −1.6‰ to +4.5‰ ($n = 24$) and −2.4‰ to +1.8‰ ($n = 13$), respectively. The studies suggest that S in the Beiya ore-forming fluids has a magma-derived source that related to Cenozoic alkaline porphyries, similar to many other porphyry-related Cu–Mo–(Au) and epithermal Pb–Zn–Ag deposits in the Jinshajiang–Red River (Ailaoshan) metallogenic belt (Xiao et al., 2011). The $\delta^{34}S$ values of sulfide separates from Luping (Fig. 9a) overlap those of Beiya (Fig. 9b), also suggesting that the source of S in the Luping ore-forming fluids is magma-related, most likely associated with the Cenozoic alkali-rich porphyries at Beiya.

5.3. Origin of ore-forming metals

Because some Pb isotopes are radiogenic, the Pb isotopic ratios need to be corrected to a consistent age in order to make comparisons between different phases (e.g., Carr et al., 1995; Haest et al., 2010; Muchez et al., 2005; Zhang et al., 2002; Zhou et al., 2013a,b,c). Sulfides have very low U and Th contents, and hence radiogenic Pb is negligible and no age correction is needed, whereas such age correction is needed for the sedimentary rocks and porphyry whole-rock data. Our C–O and S isotopic data suggest that the formation of the Luping Pb deposit is related to alkali-rich porphyries in the Beiya area, and the quartz syenite porphyry dikes are newly dated to be 36.2 ± 0.4 Ma (Fig. 7b, c). Thus, an age of 36 Ma is used to correct the Pb isotopic compositions of the

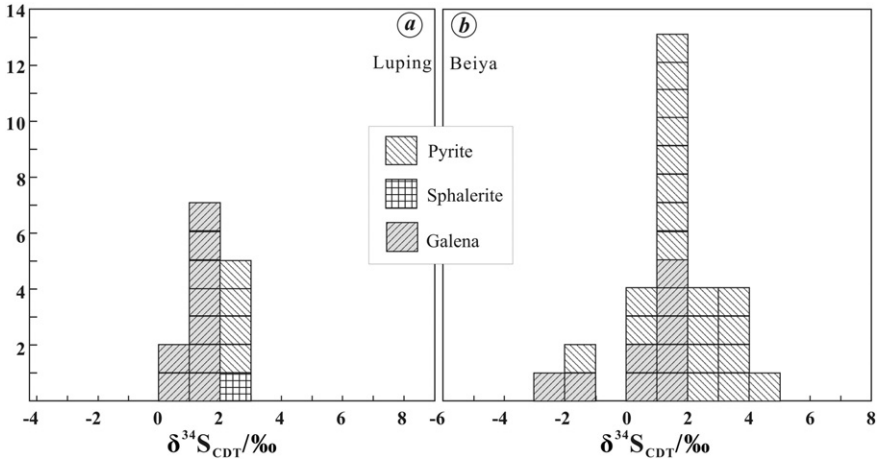

Fig. 9. a: Histogram of $\delta^{34}S_{CDT}$ values for the sulfides from Luping; b. Histogram of $\delta^{34}S_{CDT}$ values for the sulfides from Beiya. Data are from Xiao et al. (2011).

Table 5
Pb isotopic data for sulfide separates, and the sedimentary host rocks and porphyry whole-rock at Luping.

No.	Mineral/rock	$^{206}Pb/^{204}Pb$	2σ	$^{207}Pb/^{204}Pb$	2σ	$^{208}Pb/^{204}Pb$	2σ
LPD-1	Pyrite	18.653	0.002	15.699	0.002	39.055	0.005
LPD-2	Pyrite	18.632	0.002	15.657	0.002	38.923	0.005
LPD-18	Pyrite	18.667	0.002	15.684	0.001	39.023	0.003
LPD-28	Pyrite	18.675	0.002	15.696	0.002	39.084	0.005
LPD-10	Sphalerite	18.694	0.002	15.703	0.002	39.073	0.004
LPD-3	Galena	18.657	0.003	15.687	0.002	39.036	0.005
LPD-4	Galena	18.657	0.002	15.667	0.002	38.955	0.004
LPD-9	Galena	18.653	0.002	15.667	0.001	38.963	0.003
LPD-19	Galena	18.652	0.002	15.676	0.001	39.003	0.004
LPD-24	Galena	18.652	0.002	15.677	0.001	39.013	0.004
LPD-26	Galena	18.637	0.002	15.671	0.002	38.982	0.005
LPD-27	Galena	18.655	0.003	15.691	0.003	39.053	0.007
LPD-29	Galena	18.642	0.002	15.675	0.002	38.997	0.004
LPD-36	Galena	18.623	0.002	15.683	0.002	38.998	0.004
LPD-53	Limestone	18.908	0.003	15.649	0.002	38.949	0.006
ZK750-7	Dolostone	18.680	0.002	15.631	0.002	38.848	0.005
LPD-39	Limestone	18.687	0.002	15.639	0.001	38.996	0.003
ZK1861-1	Sandstone	18.659	0.002	15.634	0.001	38.976	0.004
LPD-12	Sandstone	18.771	0.002	15.624	0.001	39.095	0.004
ZK2342-5	Sandstone	18.702	0.004	15.702	0.003	39.076	0.008
ZK9090-2	Porphyry	18.639	0.002	15.677	0.002	39.008	0.004
ZK9090-3	Porphyry	18.648	0.002	15.688	0.002	39.046	0.004
ZK9090-7	Porphyry	18.641	0.002	15.677	0.002	39.005	0.005
ZK9090-8	Porphyry	18.634	0.002	15.671	0.002	38.986	0.005
ZK9090-13	Porphyry	18.642	0.002	15.672	0.002	38.995	0.005
ZK9090-14	Porphyry	18.714	0.003	15.771	0.002	39.315	0.004
ZK9090-15	Porphyry	18.612	0.003	15.636	0.003	38.884	0.007

Pb isotopic data for the sedimentary host rocks and porphyry whole-rock are age-corrected at ca. 36 Ma.

sedimentary host rocks and porphyries. Sulfide separates have Pb isotopic data lying on both sides of the upper crust and orogenic belt average evolution curves in the $^{207}Pb/^{204}Pb$ vs. $^{206}Pb/^{204}Pb$ diagram (Fig. 10; Zartman and Doe, 1981), suggesting a crustal source of Pb. Additionally, the Pb isotopic data points for the Luping sulfide separates overlap largely with those of the porphyries, but are far from the majority of the sedimentary host rocks (Fig. 10). Therefore, the source of Pb in the hydrothermal fluids was most likely porphyry-related. In addition, all Luping sulfide separates and porphyry Pb isotopic data points fall into the Beiya sulfide and porphyry fields (Fig. 10; Deng et al., 2015; Liu et al., 2015; Xiao et al., 2011), suggesting similar Pb source for the two deposits, which may have been associated with the Cenozoic alkaline porphyries that formed from partial melting of the metasomatized subcontinental lithospheric mantle (SCLM) (Deng et al., 2015; Liu et al., 2015).

5.4. Ore genesis of the Luping Pb deposit

The Beiya deposit is likely to be genetically related to the Eocene alkaline porphyry at Beiya, and is best classified as a porphyry-related Au–Fe–Cu skarn deposit (Deng et al., 2015; Xiao et al., 2011; Xu et al., 2007). The origin of metals and ore-forming fluids at Luping may have been similar to that of the Beiya deposit, as suggested by ore deposit geology, and C–O–S and Pb isotopes. Moreover, ore bodies at Luping occur as stratiform or lenticular types within tectonic breccias, and are hosted by sedimentary rocks of the Triassic Beiya and Qingtianban Formations (Figs. 3 and 4). The Pb–Au sulfide ores have banded and vein structures (Figs. 5 and 6), and occur with only minor amount of porphyry dikes. Therefore, we propose that Luping is a stratiform, bedding-plane fault-controlled epithermal Pb polymetallic deposit, genetically related to Eocene (ca. 36 Ma–31 Ma) alkaline porphyries in the Beiya area (Fig. 11). It is a newly identified mineralization type at Beiya and is likely to be a constituent of the Beiya porphyry metallogenic system. The geodynamic setting of the Luping Pb polymetallic mineralization resembles other Eocene porphyry-related Cu–Mo–(Au) and epithermal Pb–Zn–Ag deposits along the Jinshajiang–Red River (Ailaoshan) metallogenic belt (Mao et al., 2014). These deposits may have been formed in the India–Eurasia post-collisional setting (Deng et al., 2014; Hou et al., 2007; Hou and Zhang, 2015; Mao et al., 2014), when partial melting occurred in the Triassic stagnant slab that thickened the lower crust and the upper mantle, producing the alkaline magmatism and its associated mineralization (Deng et al., 2015; Liu et al., 2015).

6. Conclusions

1) New C–O–S and Pb isotopic data suggest that the Luping deposit and the Eocene alkaline porphyries are genetically linked.
2) The Luping is a newly identified stratiform, bedding-plane fault-controlled epithermal Pb polymetallic deposit in the Beiya area.
3) The Luping deposit is a part of the Beiya porphyry system that may have formed in the India–Eurasia post-collisional setting.

Conflict of interest

There is no conflict of interest.

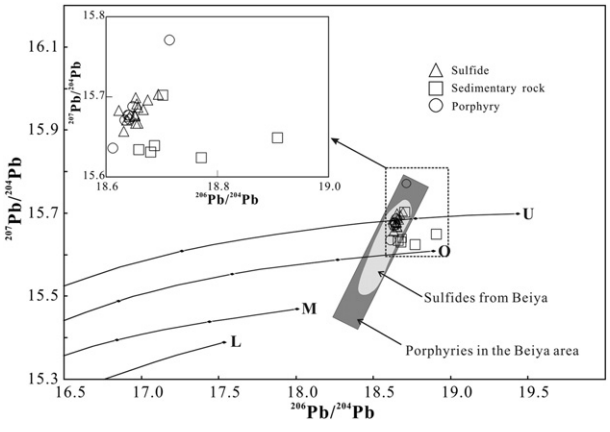

Fig. 10. Plot of $^{207}Pb/^{204}Pb$ versus $^{206}Pb/^{204}Pb$ for sulfides, sedimentary host rocks and porphyries from Luping. Trends for the Upper Crust (U), Orogenic Belt (O), Mantle (M) and Lower Crust (L) are from Zartman and Doe (1981). Data of the Beiya Au deposit are from Deng et al. (2015), Liu et al. (2015), Xiao et al. (2011) and Xu et al. (2007).

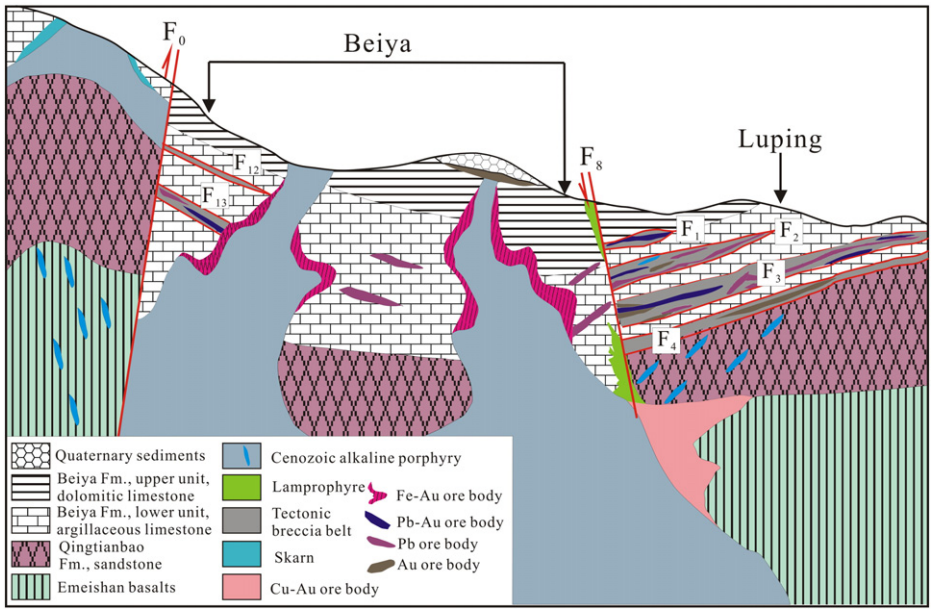

Fig. 11. Metallogenic model for the porphyry Cu–Au and epithermal Pb–Zn–Ag mineralization at Beiya (Luping). During 65 Ma–25 Ma, under the India–Eurasia post-collisional tectonics (Deng et al., 2014; Hou and Zhang, 2015; Mao et al., 2014), partial melting occurred in the Triassic stagnant slab that thickened the lower crust and the upper mantle, producing the alkaline magmatism and its associated mineralization (Deng et al., 2015; Liu et al., 2015).

Acknowledgments

The research is jointly supported by the 12th Five-Year Plan Project of State Key Laboratory of Ore Deposit Geochemistry, Chinese Academy of Sciences (No. SKLODG-ZY125-02), the National Basic Research Program of China (No. 2014CB440905) and the National Natural Science Foundation of China (Nos. 41163001 and 41402072). Thanks are given to Prof. Mei-Fu Zhou, Prof. Bor-ming Jahn and Dr. Ping-Ping Liu for useful discussion. Comments and suggestions from Prof. Franco Pirajno (Editor-in-Chief), Prof. Jing-Wen Mao (Associate Editor), Prof. Xing-Wang Xu and two anonymous reviewers have greatly enhanced the paper.

References

Basuki, N.I., Taylor, B.E., Spooner, E.T.C., 2008. Sulfur isotope evidence for thermochemical reduction of dissolved sulfate in Mississippi valley type zinc–lead mineralization, Bongara area, northern Peru. Econ. Geol. 103, 183–799.

Bath, A.B., Cooke, D.R., Friedman, R.M., Faure, K., Kamenetsky, V.S., Tosdal, R.M., Berry, R.F., 2014. Mineralization, U–Pb geochronology, and stable isotope geochemistry of the Lower Main zone of the Lorraine deposit, north-central British Columbia: a replacement-style alkalic Cu–Au porphyry. Econ. Geol. 109, 979–1004.

Cai, X., 1991. Characteristics, genesis and target prediction of Au deposit in the Beiya area, western Yunnan. Research Report, p. 51 (in Chinese).

Carr, G.R., Dean, J.A., Suppel, D.W., Heithersay, P.S., 1995. Precise lead isotope fingerprinting of hydrothermal activity associated with Ordovician to Carboniferous metallogenic events in the Lachlan fold belt of New South Wales. Econ. Geol. 90, 1467–1505.

Chaussidon, M., Albarède, F., Sheppard, S.M.F., 1989. Sulfur isotope variations in the mantle from ion microprobe analyses of micro-sulfide inclusions. Earth Planet. Sci. Lett. 92, 144–156.

Demény, A., Harangi, S.Z., 1996. Stable isotope studies on carbonate formations in alkaline basalt and lamprophyre series: evolution of magmatic fluids and magma–sediment interactions. Lithos 37, 335–349.

Demény, A., Ahijado, A., Casillas, R., Vennemann, T.W., 1998. Crustal contamination and fluid/rock interaction in the carbonatites of Fuerteventura (Canary Islands, Spain): a C, O, H isotope study. Lithos 44, 101–115.

Deng, J., Wang, Q.F., Li, G.J., Santosh, M., 2014. Cenozoic tectono-magmatic and metallogenic processes in the Sanjiang region, southwestern China. Earth-Sci. Rev. 138, 268–299.

Deng, J., Wang, Q.F., Li, G.J., Hou, Z.Q., Jiang, C.Z., Danyushevsky, L., 2015. Geology and genesis of the giant Beiya porphyry-skarn gold deposit northwestern Yangtze Block China. Ore Geol. Rev. 70, 457–485.

Dixon, G., Davidson, G.J., 1996. Stable isotope evidence for thermo chemical sulfate reduction in the Dugald River (Australia) strata-bound shale-hosted zinc–lead deposit. Chem. Geol. 129, 227–246.

Dou, S., Liu, J.S., Guo, Y.S., Yan, J., 2013. Ore mineralogical characteristics of the Luping lead polymetallic deposit in Heqing of Yunnan province and their geological implications. Acta Geosci. Sin. 34 (Suppl. 1), 87–94 (in Chinese with English abstract).

Ge, L.S., Guo, X.D., Zou, Y.L., Yang, J.H., Li, Y.J., 2002. Geology and genesis of Yao'an Au deposit related to alkali-rich magmatic rock in Yunnan province. Geol. Res. 11, 29–37 (in Chinese with English abstract).

Gray, D.R., Gregory, R.T., Durney, D.W., 1991. Rock-buffered fluid-rock interaction in deformed quartz-rich turbidite sequences, eastern Australia. J. Geophys. Res. Solid Earth 96, 19681–19704.

Haest, M., Schneider, J., Cloquet, C., Latruwe, K., Vanhaecke, F., Muchez, P., 2010. Pb isotopic constraints on the formation of the Dikulushi Cu–Pb–Zn–Ag mineralization, Kundelungu Plateau (Democratic Republic of Congo). Miner. Deposita 45, 393–410.

He, W.Y., Mo, Yu.X.H., He, X.X., Li, Z.H., Huang, Y., Su, X.K., G.S.,, 2012. Genetic types and the relationship between alkali-rich intrusion and mineralization of Beiya gold polymetallic ore field, western Yunnan Province, China. Acta Petrol. Sin. 28, 1401–1412 (in Chinese with English abstract).

He, W.Y., Mo, X.X., Yu, X.H., He, Z.H., Dong, G.C., Liu, X.B., Su, G.S., Huang, X.F., 2013. Zircon U–Pb and molybdenite Re–Os dating for the Beiya gold polymetallic deposit in the western Yunnan Province and its geological significance. Acta Petrol. Sin. 29, 1301–1310 (in Chinese with English abstract).

Hou, Z.Q., Cook, N.J., 2009. Metallogenesis of the Tibetan collisional orogen: a review and introduction to the special issue. Ore Geol. Rev. 36, 2–24.

Hou, Z.Q., Zhang, H.R., 2015. Geodynamics and metallogeny of the eastern Tethyan metallogenic domain. Ore Geol. Rev. 70, 346–384.

Hou, Z.Q., Zeng, P.S., Gao, Y.F., 2006. Himalayan Cu–Mo–Au mineralization in the eastern Indo–Asian collision zone: constraints from Re–Os dating of molybdenite. Miner. Deposita 41, 33–45.

Hou, Z.Q., Zaw, K., Pan, G.T., Mo, X.X., Xu, Q., Hu, Y.Z., Li, X.Z., 2007. The Sanjiang Tethyan metallogenesis in S.W. China: tectonic setting, metallogenic epoch and deposit type. Ore Geol. Rev. 31, 48–87.

Hu, R.Z., Bi, X.W., Shao, S., Turner, G., Burnard, P.G., 1997. Study on helium isotope composition of Cu deposit in Machangqing, Yunnan, China. Chin. Sci. Bull. 42, 1542–1545 (in Chinese with English abstract).

Hu, R.Z., Burnard, P.G., Bi, X.W., Zhou, M.F., Peng, J.T., Su, W.C., Wu, K.X., 2004. Helium and argon isotope geochemistry of alkaline intrusion-associated gold and copper deposits along the Red River–Jinshajiang fault belt, SW China. Chem. Geol. 203, 305–317.

Jemmali, N., Souissi, F., Carranza, E.J.M., Vennemann, T.W., 2013. Sulfur and lead isotopes of Guern Halfaya and Bou Grine deposits (Domes zone, northern Tunisia): implications for sources of metals and timing of mineralization. Ore Geol. Rev. 54, 17–28.

Layton–Matthews, D., Leybourne, M.I., Peter, J.M., Scott, S.D., Cousens, B., Eglington, B.M., 2013. Multiple sources of selenium in ancient seafloor hydrothermal systems: compositional and Se, S, and Pb isotopic evidence from volcanic-hosted and volcanic-sediment-hosted massive sulfide deposits of the Finlayson Lake District, Yukon, Canada. Geochim. Cosmochim. Acta 117, 313–331.

Liang, H.Y., Campbell, I.H., Allen, C.M., Sun, W.D., Yu, H.X., Xie, Y.W., Zhang, Y.Q., 2007. The age of the potassic alkaline igneous rocks along the Ailao Shan–Red River shear zone: implications for the onset age of left-lateral shearing. J. Geol. 115, 231–242.

Liu, J.M., Liu, J.J., 1997. Basin fluid genetic model of sediment-hosted micro-disseminated gold deposits in the gold-triangle area between Guizhou, Guangxi and Yunnan. Acta Miner. Sin. 17, 448–456 (in Chinese with English abstract).
Liu, Y.S., Hu, Z.C., Gao, S., Gunther, D., Xu, J., Gao, C.G., Chen, H.H., 2008. In situ analysis of major and trace elements of anhydrous minerals by LA-ICP-MS without applying an internal standard. Chem. Geol. 257, 34–43.
Liu, Y.S., Gao, S., Hu, Z.C., Gao, C.G., Zong, K.Q., Wang, D.B., 2010a. Continental and oceanic crust recycling-induced melt-peridotite interactions in the Trans-North China Orogen: U–Pb dating, Hf isotopes and trace elements in zircons from mantle xenoliths. J. Petrol. 51, 537–571.
Liu, Y.S., Hu, Z.C., Zong, K.Q., Gao, C.G., Gao, S., Xu, J., Chen, H.L., 2010b. Reappraisement and refinement of zircon U–Pb isotope and trace element analyses by LA-ICP-MS. Chin. Sci. Bull. 55, 1535–1546 (in Chinese with English abstract).
Liu, B., Liu, H., Zhang, C.Q., Mao, Z.H., Zhou, Y.M., Huang, H., He, Z.H., Su, G.S., 2015. Geochemistry and geochronology of porphyries from the Beiya gold-polymetallic orefield, western Yunnan, China. Ore Geol. Rev. 69, 360–379.
Lu, Y.J., Kerrich, R., Cawood, P.A., McCuaig, T.C., Hart, C.J.R., Li, Z.X., Hou, Z.Q., Bagas, L., 2012. Zircon SHRIMP U–Pb geochronology of potassic felsic intrusions in western Yunnan, SW China. Constraints on the relationship of magmatism to the Jinshajiang suture. Gondwana Res. 22, 737–747.
Mao, J.W., Wang, Y.T., Li, H.M., Pirajno, F., Zhang, C.Q., Wang, R.T., 2008. The relationship of mantle-derived fluids to gold metallogenesis in the Jiaodong Peninsula: evidence from D–O–C–S isotope systematics. Ore Geol. Rev. 33, 361–381.
Mao, J.W., Zhang, J.D., Pirajno, F., Ishiyama, D., Su, H.M., Guo, C.L., Chen, Y.C., 2011. Porphyry Cu–Au–Mo-epithermal Ag–Pb–Zn-distal hydrothermal Au deposits in the Dexing area, Jiangxi province, East China—a linked ore system. Ore Geol. Rev. 43, 203–216.
Mao, J.W., Pirajno, F., Lehmann, B., Luo, M.C., Berzina, A., 2014. Distribution of porphyry deposits in the Eurasian continent and their corresponding tectonic settings. J. Asian Earth Sci. 79, 576–584.
Moura, M.A., Botelho, N.F., Olivo, G.R., Kyser, K., Pontes, R.M., 2014. Genesis of the Proterozoic Mangabeira tin-indium mineralization, Central Brazil: evidence from geology, petrology, fluid inclusion and stable isotope data. Ore Geol. Rev. 60, 36–49.
Muchez, P., Slobodník, M., Viaene, W.A., Keppens, E., 1995. Geochemical constraints on the origin and migration of paleo-fluids at the northern margin of the Variscan foreland, southern Belgium. Sediment. Geol. 96, 191–200.
Muchez, P., Heijlen, W., Banks, D., Blundell, D., Boni, M., Grandia, F., 2005. Extensional tectonics and the timing and formation of basin-hosted deposits in Europe. Ore Geol. Rev. 27, 241–267.
Ohmoto, H., Goldhaber, M.B., 1997. Sulfur and carbon isotopes. In: Barnes, H.L. (Ed.), Geochemistry of Hydrothermal Ore Deposits, 3rd ed. Wiley and Sons, New York, pp. 517–611.
Ohmoto, H., Rye, R.O., 1979. Isotopes of sulfur and carbon. In: Barnes, H.L. (Ed.), Geochemistry of Hydrothermal Ore Deposits, 2rd ed. Wiley and Sons, New York, pp. 509–567.
Ohmoto, H., Kaiser, C.J., Geer, K.A., 1990. Systematics of sulphur isotopes in recent marine sediments and ancient sediment-hosted base metal deposits. In: Herbert, H.K., Ho, S.E. (Eds.), Stable Isotopes and Fluid Processes in Mineralization 23. Geol. Dep. Univ. Extens. Univ., Western Australia, pp. 70–120.
Palinkaš, S.S., Palinkaš, L.A., Renac, C., Spangenberg, J.E., Lüders, V., Molnar, F., Maliqi, G., 2013. Metallogenic model of the Trepča Pb–Zn–Ag skarn deposit, Kosovo: evidence from fluid inclusions, rare earth elements, and stable isotope data. Econ. Geol. 108, 135–162.
Pass, H.E., Cooke, D.R., Davidson, G., Maas, R., Dipple, G., Rees, C., Ferreira, L., Taylor, C., Deyell, C.L., 2014. Isotope geochemistry of the northeast zone, Mount Polley alkalic Cu–Au–Ag porphyry deposit, British Columbia: a case for carbonate assimilation. Econ. Geol. 109, 859–890.
Peng, Z., Watanabe, M., Hoshino, K., Sueoka, S., Yano, T., Nishido, H., 1998. The Machangqing copper–molybdenum deposits, Yunnan, China: an example of Himalayan porphyry-hosted Cu–Mo mineralization. Miner. Petrol. 63, 95–117.
Qian, X., Li, Z., Bo, J., 2000. A preliminary study on the genetic mechanism of Yaoan Au deposit. Yunnan Geol. 21, 42–49 (in Chinese with English abstract).
Taylor, J.H.P., Frechen, J., Degens, E.T., 1967. Oxygen and carbon isotope studies of carbonatites from the Laacher See District, West Germany and the Alno District Sweden. Geochim. Cosmochim. Acta 31, 407–430.
Veizer, J., Hoefs, J., 1976. The nature of $^{18}O/^{16}O$ and $^{13}C/^{12}C$ secular trends in sedimentary carbonate rocks. Geochim. Cosmochim. Acta 40, 1387–1395.
Wang, X., Metcalfe, I., Jian, P., He, L., Wang, C., 2000. The Jinshajiang–Ailaoshan suture zone: tectono-stratigraphy, age and evolution. J. Asian Earth Sci. 18, 675–690.
Wang, J.H., Yin, A., Harrison, T.M., Grove, M., Zhang, Y.Q., Xie, G.H., 2001. A tectonic model for Cenozoic igneous activities in the eastern Indo–Asian collision zone. Earth Planet. Sci. Lett. 88, 123–133.
Wu, K.X., Hu, R.Z., Bi, X.W., Peng, J.T., 2010. An oxygen and carbon isotope study on the formation mode of calcite in Beiya gold deposit, west Yunnan Province, China. Acta Miner. Sin. 30, 463–469 (in Chinese with English abstract).
Xiao, X.N., Yu, X.H., Mo, X.X., Huang, X.K., Li, Y., 2011. Geochemical characteristics of metallogenesis in the gold polymetallic deposit in Beiya, western Yunnan province. Geol. Prospect. 47, 170–179 (in Chinese with English abstract).
Xu, X.W., Cai, X.P., Song, B.C., 2006. Petrologic, chronological and geochemistry characteristics and formation mechanism of alkaline porphyries in the Beiya gold district, western Yunnan. Acta Petrol. Sin. 22, 631–642 (in Chinese with English abstract).
Xu, X.W., Cai, X.P., Xiao, Q.B., Peters, S.G., 2007. Porphyry Cu–Au and associated polymetallic Fe–Cu–Au deposits in the Beiya area, western Yunnan Province, South China. Ore Geol. Rev. 31, 224–246.
Xu, L.L., Bi, X.W., Hu, R.Z., Zhang, X.C., Su, W.C., Qu, W.J., Hu, Z.C., Tang, Y.Y., 2012. Relationships between porphyry Cu–Mo mineralization in the Jinshajiang–Red River metallogenic belt and tectonic activity: constraints from zircon U–Pb and molybdenite Re–Os geochronology. Ore Geol. Rev. 48, 460–473.
Xu, L.L., Bi, X.W., Hu, R.Z., Tang, Y.Y., Jiang, G.H., Qi, Y.Q., 2014. Origin of the ore-forming fluids of the Tongchang porphyry Cu–Mo deposit in the Jinshajiang–Red River alkaline igneous belt, SW China: constraints from He, Ar and S isotopes. J. Asian Earth Sci. 79, 884–894.
Yang, Y., Hou, Z., Huang, D., Qu, X., 2002. Collision orogenic processes and magmatic metallogenic system in Zhongdian arc. Acta Geosci. Sin. 23, 17–24 (in Chinese with English abstract).
Zartman, R.E., Doe, B.R., 1981. Plumbotectonics—the model. Tectonophysics 75, 135–162.
Zaw, K., Peters, S.G., Cromie, P., Burrett, C., Hou, Z., 2007. Nature, diversity of deposit types and metallogenic relations of South China. Ore Geol. Rev. 31, 3–47.
Zhang, Y.Q., Xie, Y.W., Li, X.H., Qiu, H.N., Zhao, Z.H., Liang, H.Y., Zhong, S.L., 2000. Chronology and Nd–Sr isotopes of the Ailaoshan–Jinshajiang alkali-rich intrusion. Sci. China Earth Sci. 27, 289–293.
Zhang, Q., Liu, J.J., Shao, S.X., 2002. An estimate of the lead isotopic compositions of upper mantle and upper crust and implications for the source of lead in the Jinding Pb–Zn deposit in western Yunnan, China. Geochem. J. 36, 271–287.
Zhou, J.X., Huang, Z.L., Zhou, M.F., Li, X.B., Jin, Z.G., 2013a. Constraints of C–O–S–Pb isotope compositions and Rb–Sr isotopic age on the origin of the Tianqiao carbonate-hosted Pb–Zn deposit, SW China. Ore Geol. Rev. 53, 77–92.
Zhou, J.X., Huang, Z.L., Bao, G.P., 2013b. Geological and sulfur–lead–strontium isotopic studies of the Shaojiwan Pb–Zn deposit, southwest China: implications for the origin of hydrothermal fluids. J. Geochem. Explor. 128, 51–61.
Zhou, J.X., Huang, Z.L., Yan, Z.F., 2013c. The origin of the Maozu carbonate-hosted Pb–Zn deposit, southwest China: constrained by C–O–S–Pb isotopic compositions and Sm–Nd isotopic age. J. Asian Earth Sci. 73, 39–47.
Zhou, J.X., Huang, Z.L., Zhou, M.F., Zhu, X.K., Muchez, P., 2014a. Zinc, sulfur and lead isotopic variations in carbonate-hosted Pb–Zn sulfide deposits, southwest China. Ore Geol. Rev. 58, 41–54.
Zhou, J.X., Huang, Z.L., Lv, Z.C., Zhu, X.K., Gao, J.G., Mirnejad, H., 2014b. Geology, isotope geochemistry and ore genesis of the Shanshulin carbonate-hosted Pb–Zn deposit, southwest China. Ore Geol. Rev. 63, 209–225.
Zhu, X.P., Mo, X.X., White, N.C., Zhang, B., Sun, M.X., Wang, S.X., Zhao, S.L., Yang, Y., 2013. Petrogenesis and metallogenic setting of the Habo porphyry Cu–(Mo–Au) deposit, Yunnan, China. J. Asian Earth Sci. 66, 188–203.